

PROPELLERS FOR THE NEWBURY MANFLIER

by F G Irving, Imperial College, London

Paper Presented at the Royal Aeronautical Society Symposium on "Man Powered Flight - The Way Ahead" held on 7 February 1977.

Propellers for the Newbury Manflier

by F.G. Irving

Introduction

This paper describes the design of the propellers for the Newbury Manflier, a two-man aircraft conceived by Rear-Admiral H.C.N. Goodhart. The propellers have to supply the propulsion both during the take-off run and in the air, and therefore have to be designed around two sets of operating conditions. Also, in the absence of any significant flywheel in the drive system, they are subject to quite large cyclic fluctuations in torque arising from the pedalling action.

On paper, the final design meets all the above desiderata and has a propulsive efficiency of 0.88 at the cruise condition.

Performance Requirements. The requirements for *each* propeller were as follows:

Diameter: 9 ft (2.744 m),

Hub diameter: 0.5 ft (0.152 m).

	V	Thrust power,	Thrust,	
	m/s	watts	N	RPM
Take off and climb	6.7	300	44.8	
Straight cruise	7.6	170	22.4	180
Turning (inner prop)	7.2	160	22.2	
Turning (outer prop)	8.1	180	22.2	

Max torque = 1.6 x mean torque.

Preliminary Considerations. Propellers for man-powered aircraft are distinguished by the low Reynolds numbers at which the blade sections operate and by their extremely low disc loading.

Consequences of the low R_e ($\sim 10^5$) are that reliable section data are rare, that section profile drag coefficients are likely to be high (~ 0.03) and that the consequential losses are likely to be significant.

For the present purposes, Professor F.X. Wortmann of Stuttgart was kind enough to provide data on several sections at Reynolds numbers between 2×10^4 and 8×10^4 . The most useful-looking section (largely because the lower surface was flat) was designated "Jedelski Fahne 0%" but, in the event, ordinates were not available. The final choice was NACA 2412: the profile is everywhere convex, the performance is quite good at low R_e and Ref.1 gives data for $R_e = 7 \times 10^5$.

Interpolation between the NACA and Dr. Wortmann's data therefore enabled estimates of the performance for $8 \times 10^4 \leq R_e \leq 3 \times 10^5$ to be derived. Section data are shown in Fig.1.

The low disc loading means that the axial induced velocities are very low, the Froude efficiency is therefore high, and the shape of the thrust distribution curve has little effect on the Froude efficiency.

The initial design. Propellers are often designed so as to achieve the maximum possible efficiency at some design condition. Various approximate criteria exist to determine the optimum distribution of circulation along the blades. Applying a rather more elaborate version of the criterion of Ref.2 indicated that the resulting geometry was quite impracticable.

Since the distribution of circulation, and hence thrust, appeared to be of relatively little consequence, it seemed

reasonable to adopt a rather more cavalier approach and to choose a constant blade chord and -for the initial calculations - a constant lift coefficient.

Some more rough calculations suggested that two blades with a chord of 4.5 in and a lift coefficient of 0.5 would satisfy the cruise condition. (At this juncture, I must apologize for the mixture of units. Since the propeller dimensions were originally stated in feet, it was convenient to use Imperial units for the geometry and hence for the aerodynamic calculations too).

The blade angles were obtained and the performance was analysed by the method described in Appendix III. For this design, the theoretical thrust was 5.23 lbf (23.26 N) against the design cruise figure of 5.03 lbf (22.37 N). This degree of agreement was felt to be good enough: it meant that the cruise thrust would occur at some RPM slightly less than 180.

Although, presented here as a first approximation, this propeller was in fact the third.

Further development of the design. It was clear from Fig.2 that this propeller design would satisfy the cruise condition. Assuming the maximum and minimum torques to be as shown, both could be accommodated within the calculated operating range and the blades would not stall. Since a plot of Q against T for this condition was substantially linear, the variations in torque produced corresponding variations in thrust and the mean figures were not significantly affected.

However, it became clear that the mean climb thrust was likely to lead to fairly high blade lift coefficients. From the foregoing calculations, it was a simple matter to pick out the local values of blade C_L corresponding to the climb value of J , as shown in Fig.3(a). It will be seen that the peak lift coefficient is about 1.0, leading to severe danger of local stalling when the torque variations are applied.

It was therefore decided to redesign the propeller around the climb condition. The blade chord was increased to 6 in, with a uniform C_L of 0.64 when climbing. The intention was also to attempt some reduction in the climbing RPM from the previous 198. The choice of C_L was, of course, the result of a few preliminary estimates. The intention was to accept that, in the cruise condition, the local lift coefficients would be quite low, much lower than those corresponding to two-dimensional $(L/D)_{max}$.

Again, the blade angles were calculated and the performance derived by the method of Appendix III. This design produced the required climb thrust at 194 RPM and the cruise thrust at 185 RPM. It obviously required a little more refinement but, in view of the distribution of C_L along the blades in the cruise condition, there was little point in doing so (Fig. 3(b)). The very low values although the inner half of the blades indicated that, when the applied torque was a minimum, these parts of the blades would probably achieve a negative lift coefficient, leading to a severe reduction in the overall average efficiency.

Either of these two designs would have been reasonably satisfactory if the input torque had been uniform but the lack of uniformity was likely to produce the following effects:

1st Layout. Chord = 4.5 in, blade $C_L = 0.5$ at cruise. Blades likely to stall on climb.

2nd Layout. Chord = 6 in, blade $C_L = 0.64$ at climb. Blades likely to achieve negative lift coefficients at $r < 2$ ft during cruise.

The final design. It was clear from these initial layouts that the use of constant lift coefficient along the blades at one design condition represented an undesirable constraint. A gradation of lift coefficient with radius was therefore desired at the cruise condition, such that, in the climb condition, the high peak C_L of the first layout was to be appreciably flattened-out.

Obviously, there was endless scope for minor local re-adjustments. The procedure actually adopted was relatively crude. The root C_L was taken to be 0.25 and the tip value 0.375, the chord again being 6 in. A reasonable-looking but arbitrary curve was then drawn between these points to produce smoothly-varying intermediate values. In fact, the cruise thrust was then a little low, so all the local lift coefficients were increased by 8% in the final design.

Again, this design was investigated by the methods of Appendix III. Fig.4 shows the blade angle as a function of radius; Fig.3(c) shows the gradation of C_L along a blade in both conditions of flight; Fig.5 shows the dimensionless characteristics and Fig. 6 plots thrust, torque and shaft power as functions of RPM at the two forward speeds.

Comments on this design. As Fig.6(a) indicates, if the shaft torque varies by $\pm 60\%$ from the mean value, and if the inertia of the system is negligible, then the climb involves operation over practically the full working range of advance ratio. The steady-state efficiencies are then:

	J	η
Min torque	0.95	0.87
Mean torque	0.78	0.89
Max torque	0.65	0.84.

The actual efficiencies will be less than those tabulated because "starting vortices" will be generated as the blade lift coefficients alter.

Fig.6(b) indicates that the range of advance ratio in the cruise condition will be 0.84 to 1.03. The latter figure is slightly outside the intended operating range and may lead to slightly negative lift coefficients over a part of the blade (from $r = 0.75$ ft to $r = 2$ ft). However, a little, extrapolation suggests that even in this condition the steady-state efficiency should not fall below 0.75. The efficiencies become:

	J	η
Min torque	1.03	0.75
Mean torque	0.93	0.88
Max torque	0.84	0.90

In practice it should be possible to improve upon the minimum torque figure. If the pilots can achieve a minimum torque of 60% of the mean (as opposed to 40%), the maximum J becomes 1.00 and the corresponding efficiency 0.81. In the cruise condition, each pilot is producing only 185 watts (0.25 HP), so he should not find it too difficult to achieve a more uniform torque than in the climb condition. In any case, the figure of $\pm 60\%$ variation in torque was simply an intuitive estimate and the above figures take no account of the inertia of the system, small though it may be.

Effect of finite number of blades. The equations presented in Appendix II implicitly assume a large number of blades and hence uniform conditions across any section of the slipstream. The effect of a finite number of blades (two, in the present case) is to produce a corresponding number of helical vortex sheets. Conditions in the slipstream are no longer uniform: additional tip losses occur and the distribution of circulation along the blades is modified, compared with conditions corresponding to an infinite number of blades.

Approximate Calculations based on Ref.2 suggest that the loss in Froude efficiency due to the former effect is of the order of 0.6%, whilst the latter effect is quite negligible. Efficiencies quoted elsewhere in this paper have not been corrected for tip effects.

General Remarks and Conclusion

The propeller for the Newbury Manflier are required to operate over a wide range of conditions. Not only is the mean climb thrust twice that required for the cruise but, assuming a torque varying by $\pm 60\%$ from the mean, the ratio of maximum torque during the climb to minimum torque during the cruise is of the order of 6.

With a fixed-pitch propeller, it is very difficult to accommodate such a wide range of conditions: on the one hand, the blades may stall whilst climbing or, on the other hand, they may have local temporary regions of negative

lift whilst cruising, leading to a loss of efficiency. In this case, it was decided to risk a possible excursion into the latter regime.

There are, of course, other design possibilities, such as varying the chord along the blade although, at first sight, there seems to be little advantage in doing so. The best solution by far would be a variable-pitch propeller, either by some arrangement of flexible blades or a two-position mechanical arrangement. Alas, either would require much more design effort than the propellers described here.

References

1. Loftin, L.K. and Smith, H.A. "Aerodynamic Characteristics of 15 NACA Airfoil Sections at Seven Reynolds Numbers from 0.7×10^6 to 9.0×10^6 ." NACA Tech. Note 1945.
2. W.F. Durand (Ed). "Aerodynamic Theory, Vol. IV" Div. L "Aeroplane Propellers" by H. Glauert. Durand Reprinting Committee, California, 1943.

Appendix I

Symbols and Definitions

a	=	axial induced velocity factor (see Fig.7).
a'	=	circumferential induced velocity factor (see Fig.7).
B	=	number of blades.
C	=	local blade chord.
C_L	=	local blade lift coefficient.
C_D	=	local blade drag coefficient.
C_Q	=	torque coefficient $(Q/\rho N^2 D^5)$.
C_T	=	thrust coefficient $(T/\rho N^2 D^4)$.
D	=	propeller diameter.
J	=	advance ratio (V/ND) .
N	=	rotational speed (revs/s) = $\Omega/2\pi$.
Q	=	propeller torque.
R	=	radial distance along blade.
R_e	=	Reynolds number, $\rho Vc/\mu$.
T	=	propeller thrust.
V	=	forward speed.
x	=	dimensionless radius, r/D .
α	=	local blade incidence.
γ	=	$\tan^{-1}(C_D/C_L)$
η	=	propeller efficiency.
ϕ	=	airflow angle, $\tan^{-1}[V(l+a)/\Omega r(l-a')]$.
ϕ_B	=	blade angle, $(\phi+\alpha)$.
μ	=	viscosity of air.
Ω	=	angular velocity of propeller.
ρ	=	air density.
σ	=	local propeller solidity, $cB/2\pi r$.

Appendix II

Propeller Equations

The usual expressions derived from vortex-plus-blade-element theory are listed below. The notation is that of Appendix I.

$$a/(1+a) = (C_L \sigma / 4) \cos(\phi+\gamma) / \cos \gamma \sin^2 \phi. \quad (1)$$

$$a'/(1-a') = (C_L \sigma / 2) \sin(\phi+\gamma) / \cos \gamma \sin 2\phi \quad (2)$$

$$\begin{aligned} \tan \phi &= [(1+a)/(1-a')] [J/2\pi x] \\ &= [(1+a)/(1-a')] [V/\Omega r] \end{aligned} \quad (3)$$

$$dC_T/dx = 4\pi J^2 x a(1+a) \quad (4)$$

$$dC_Q/dx = 8\pi^2 J x^3 a'(1+a). \quad (5)$$

$$\eta = C_T J / 2\pi C_Q \quad (6)$$

Appendix III

Procedure for the Design and Analysis of a Propeller

1. The blade was divided into suitable elements. In the present case, radial increments of 3 in. were taken up to $r = 1$ ft and increments of 6 in. beyond that radius.
2. At each radial station, the velocity $\sqrt{(V^2 + \Omega^2 r^2)}$ was calculated for the cruise condition, in order to estimate local Reynolds numbers.
3. Having decided the local lift coefficient and Reynolds number, the local profile drag coefficient was estimated from the curves of the section characteristics by interpolation. Hence γ at each station.
4. An initial estimate of the local airflow angle ϕ was made. The accuracy of the estimate is not really important but $\tan^{-1}(V/\Omega r)$ was the obvious value to use.
5. By means of an iteration process, the local airflow angle ϕ was then obtained accurately, as follows:
 - a) Using the initial value of ϕ , a and a' can be derived from equations (1) and (2) respectively, since all other quantities on their RHS's are known.
 - b) From these values of a and a' , a better estimate of ϕ was obtained from equation (3).
 - c) This was used in equations (1) and (2) to obtain better values of a and a' : and so on.

This calculation can be done very conveniently on a Hewlett-Packard HP 25 calculator using a 48-step program. The outputs are

$(1 + a)$, $1/(1 - a')$, and the next ϕ . Insufficient steps were available to insert a conditional branching routine, so the iteration was performed by repeating the sequence until ϕ was displayed to the desired order of accuracy, usually 0.01° . Three iterations were normally sufficient, taking about 30 sec total.

6. Knowing a corresponding to the local C_L and the local Reynolds number, the local blade angle ϕ_B was simply $(\phi + \alpha)$.
7. A check was then made to see whether the desired thrust had been obtained. From equation (4) and the final value of a derived from 5(c) above, dC_T/dx can be found for each element. Numerical integration gave C_T and hence the thrust.

If the desired thrust was not obtained, the blade chord and/or the lift coefficient were adjusted until reasonable agreement was obtained.

8. The performance of the propeller was then analysed as follows:

For each blade station a series of incidences α were chosen, covering a range of C_L from some low value to near the stall. For each incidence, ϕ ($=\phi_B - \alpha$), C_L and C_D were obtained. In fact, the variations of R_e are not great for any one element, and the cruise R_e was used for all the calculations involving section characteristics.

Hence, for each blade station, all the quantities on the RHS's of equations (1) and (2) had been obtained and thus a and a' could be found.

From equations (3), (4) and (5) the advance ratio J and the thrust and torque coefficient gradings, dC_T/dx and dC_Q/dx were obtained.

Again, all of the above calculations were conveniently programmed on to an HP-25.

Curves of dC_T/dx were plotted against J for each blade station. (Fig. 8) .

Hence, for a series of values of J , dC_T/dx was plotted as a function of x , the dimensionless radius (Fig. 9).

By numerical integration, C_T was obtained as a function of J .

By a similar process, C_Q was also obtained as a function of J , and hence the overall efficiency η from equation (6).

The curves of C_T , C_Q and η (e.g. Fig-5) as functions of J form a complete description of the propeller characteristics in dimensionless terms. For the present purposes it is convenient to convert these curves to plots of thrust, torque and shaft power as functions of RPM for the two forward speeds corresponding to the climb and cruise conditions (Figs. 6(a) and (b)).

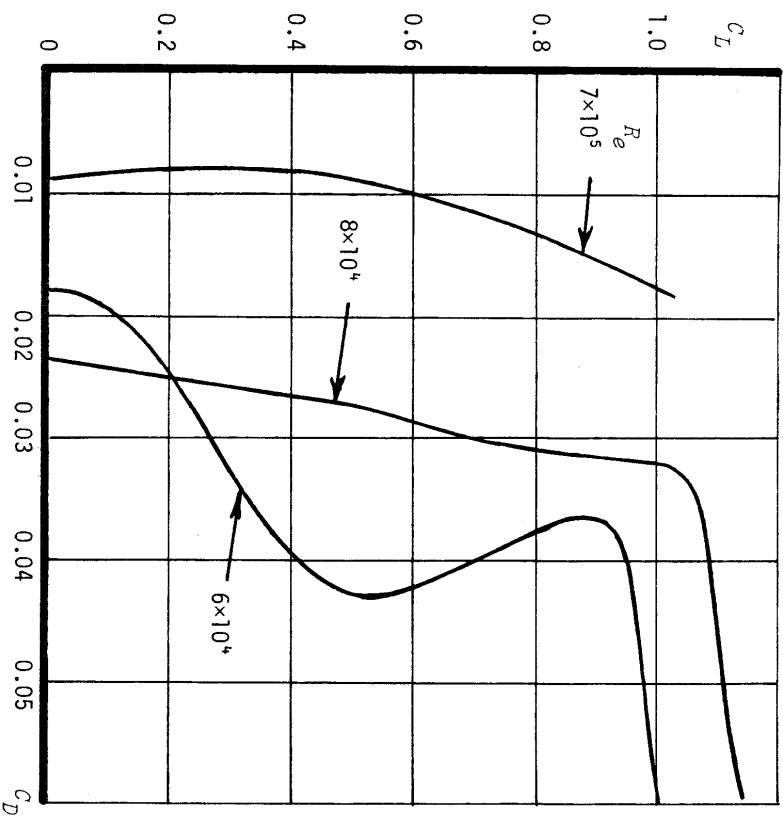
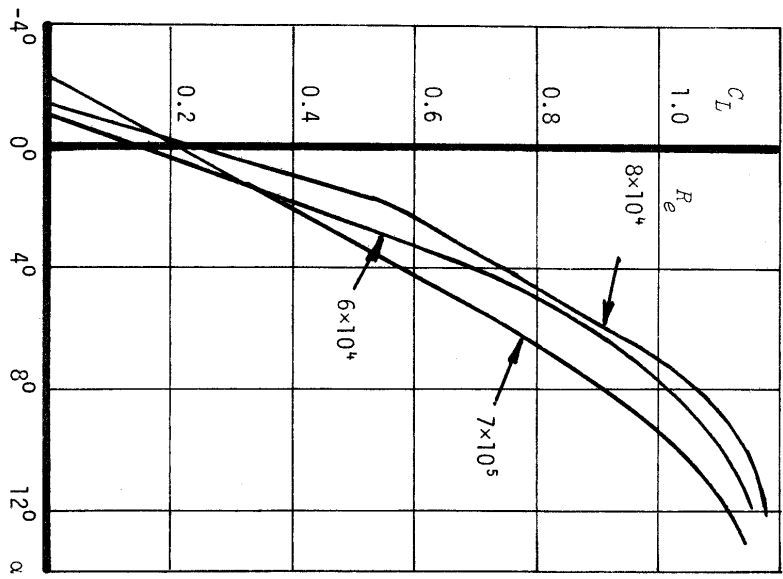


Fig. 1 Aerodynamic characteristics of the NACA 2412 aerofoil section at low Reynolds numbers.

Fig. 2
 Initial Design
 (blade chord: 4.5",
 cruise C_L : 0.5).
 Curves of thrust
 and torque vs RPM
 for the cruise
 condition.

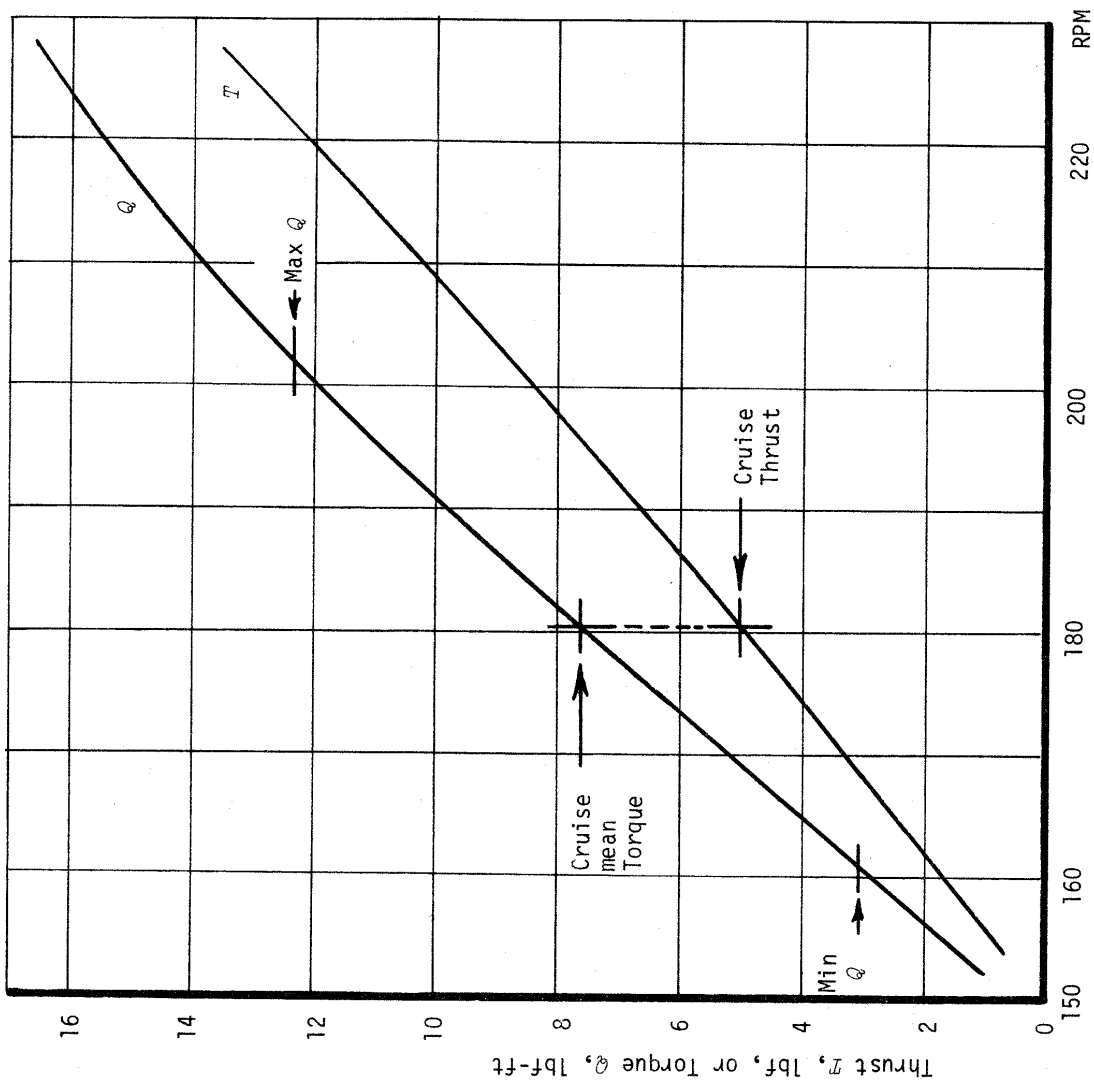
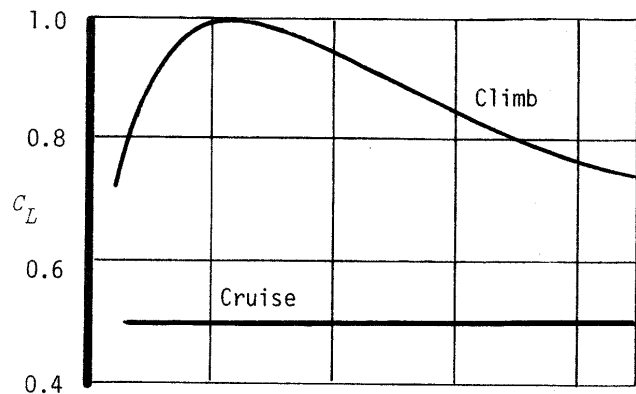
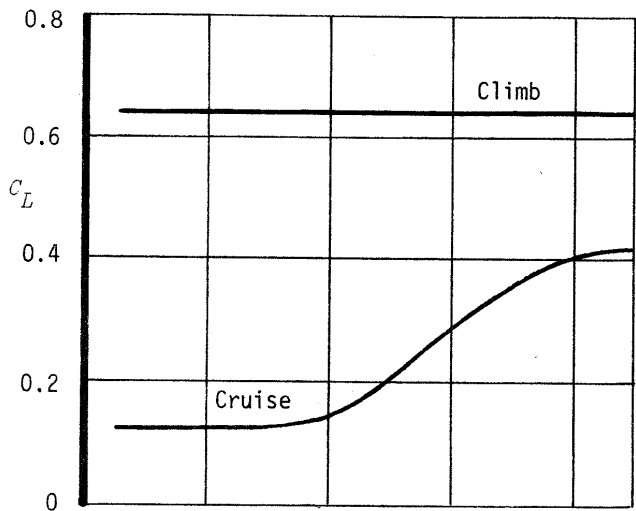


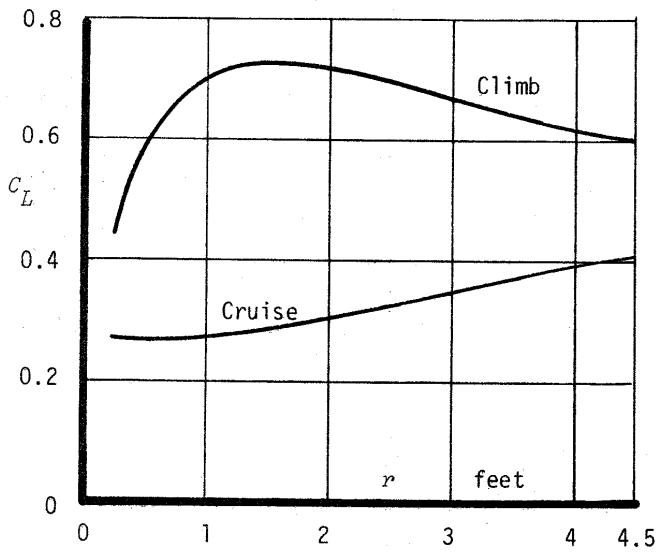
Fig. 3 Distributions of lift coefficient along the blades.



3(a) Initial design.
(Blade chord:
4.5")



3(b) Second design.
(Blade chord:
6.0")



3(c) Final design.
(Blade chord:
6.0")

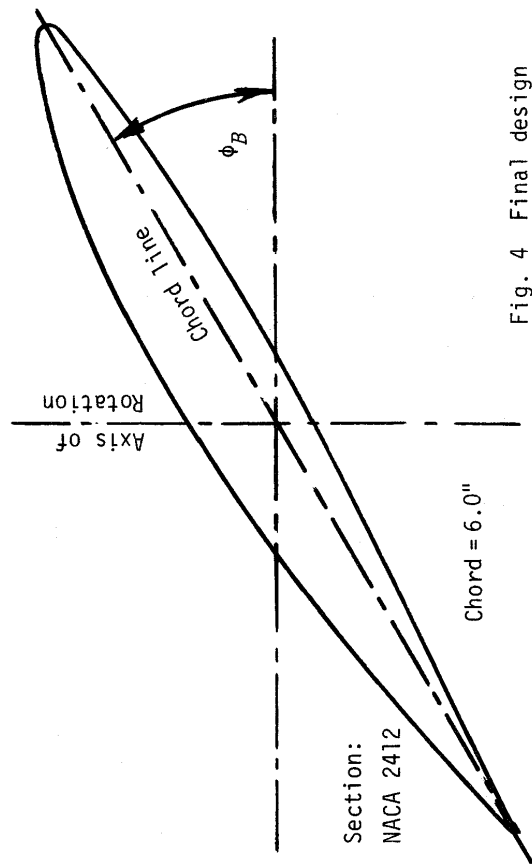
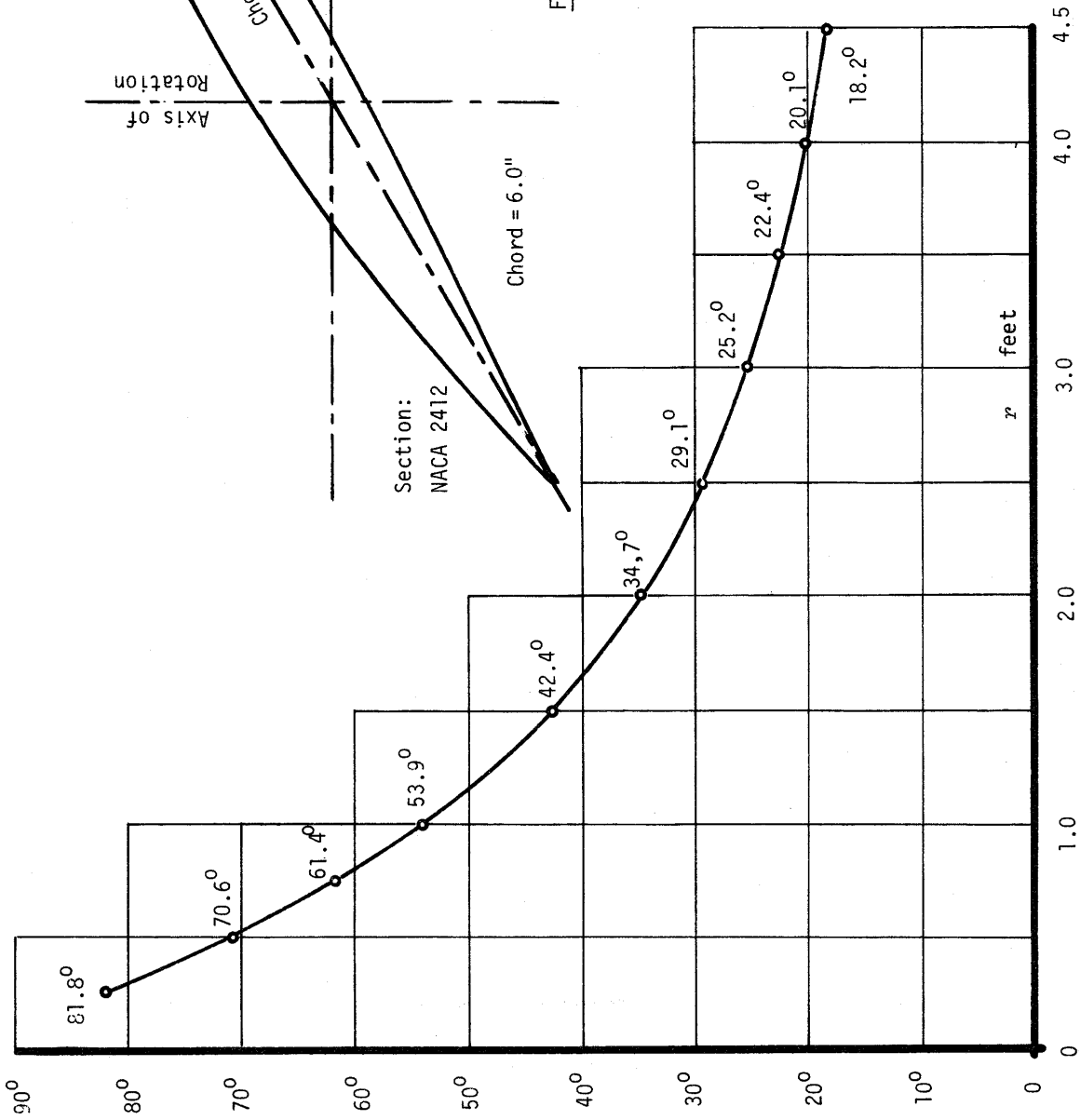


Fig. 4 Final design blade angles.

Fig. 5 Dimensionless characteristics of the final design: curves of thrust coefficient, torque coefficient and efficiency vs advance ratio.

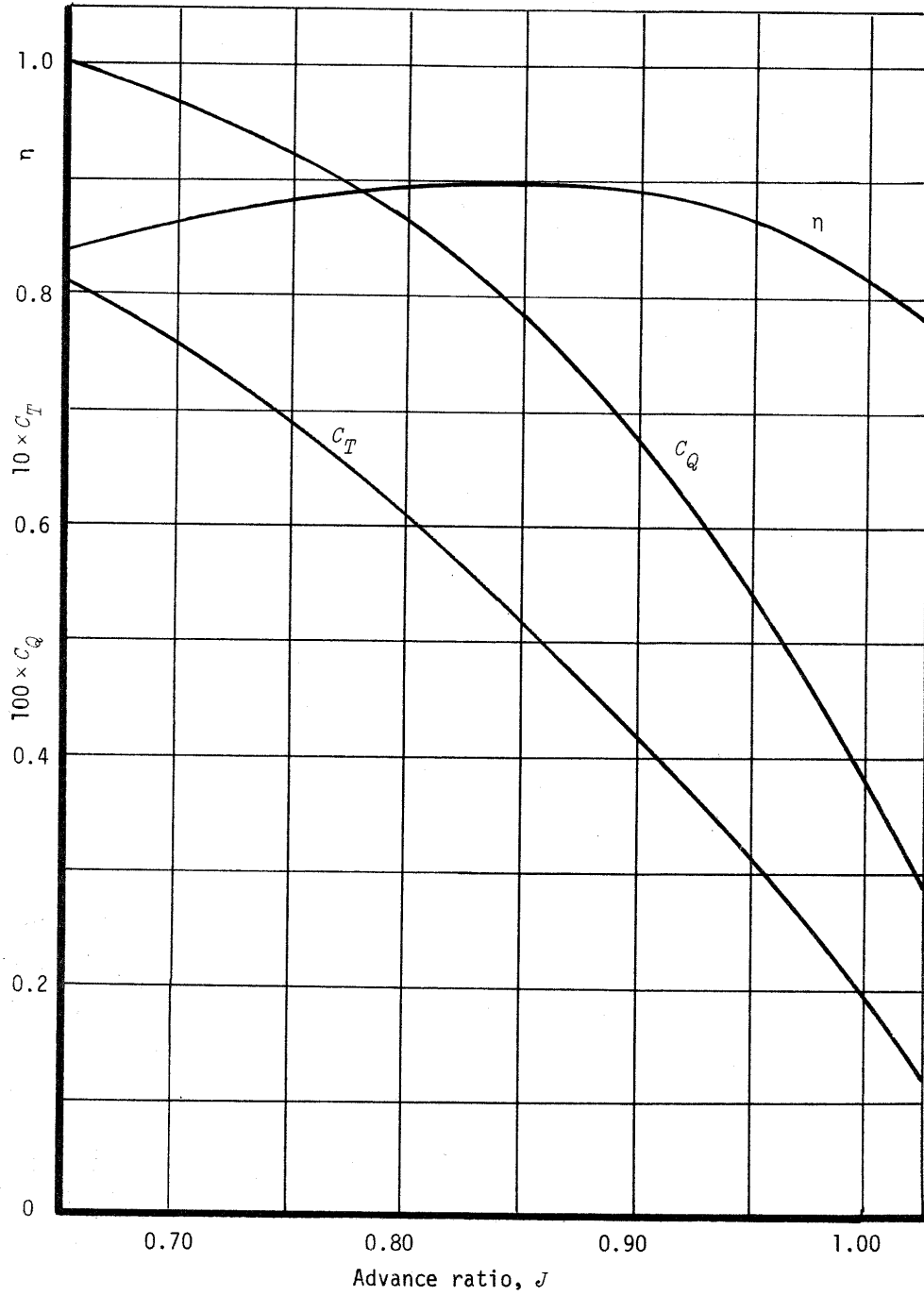


Fig. 6(a) Final design: thrust, torque and shaft power vs RPM for the climb condition.

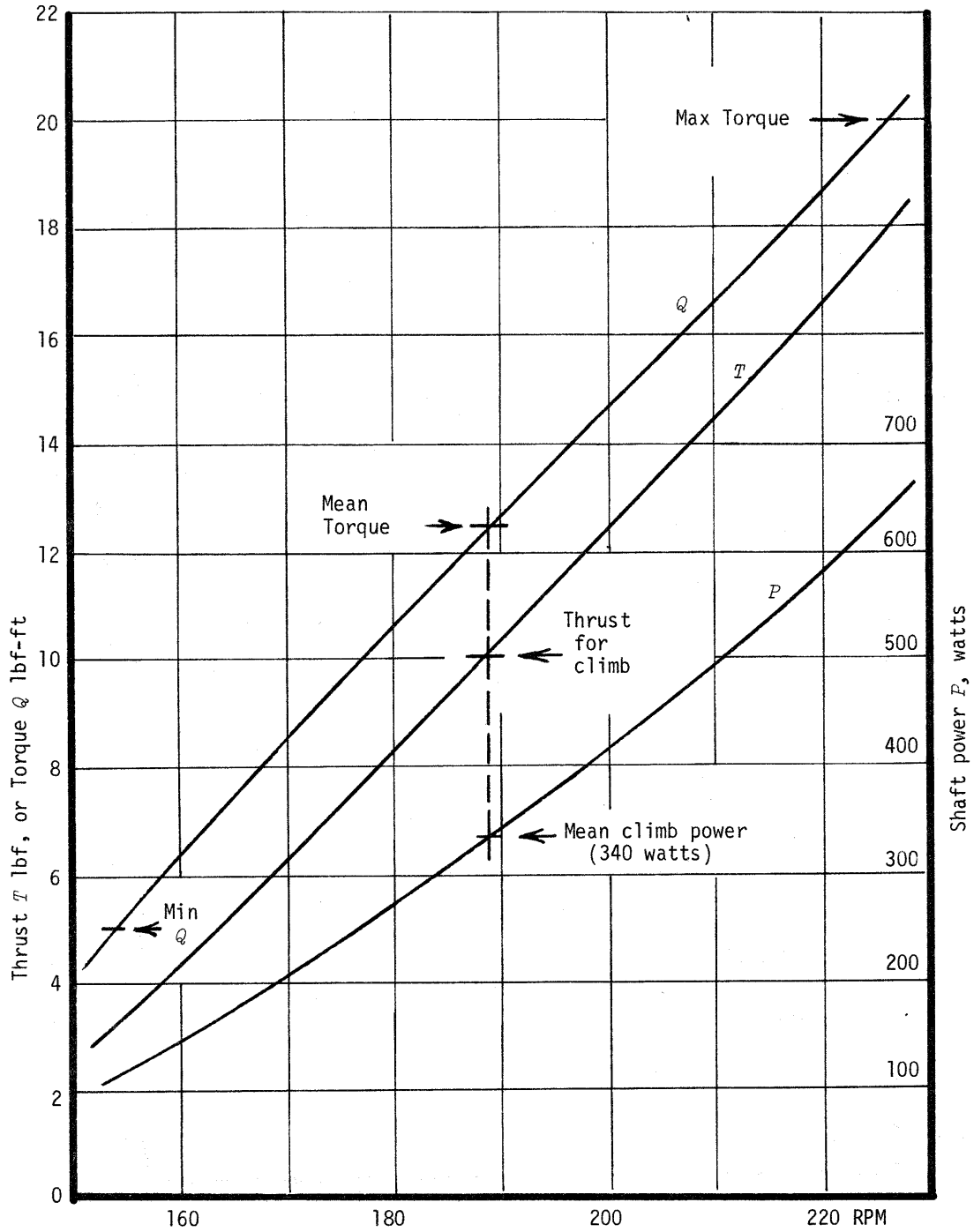


Fig. 6(b) Final design: thrust, torque and shaft power vs RPM for the cruise condition.

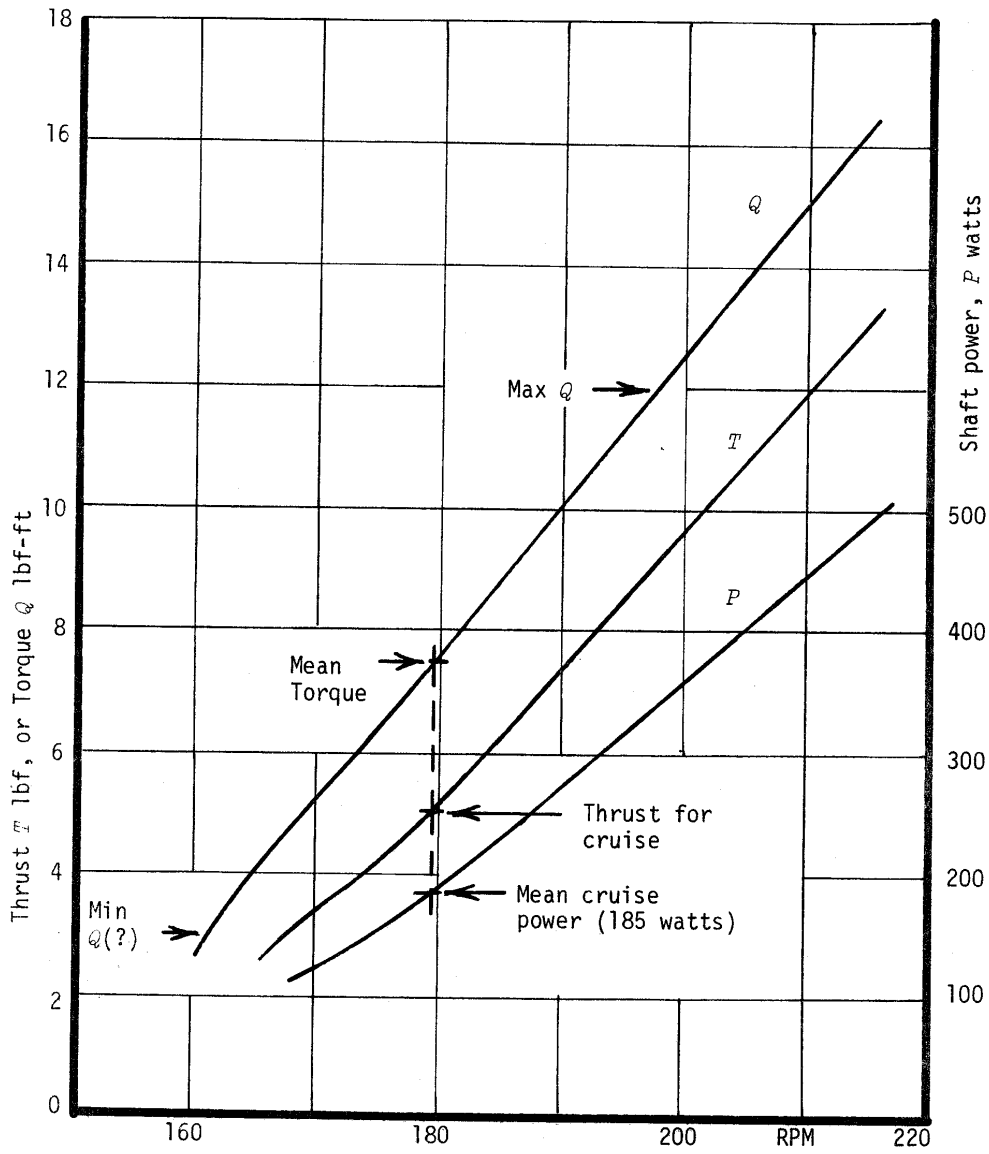
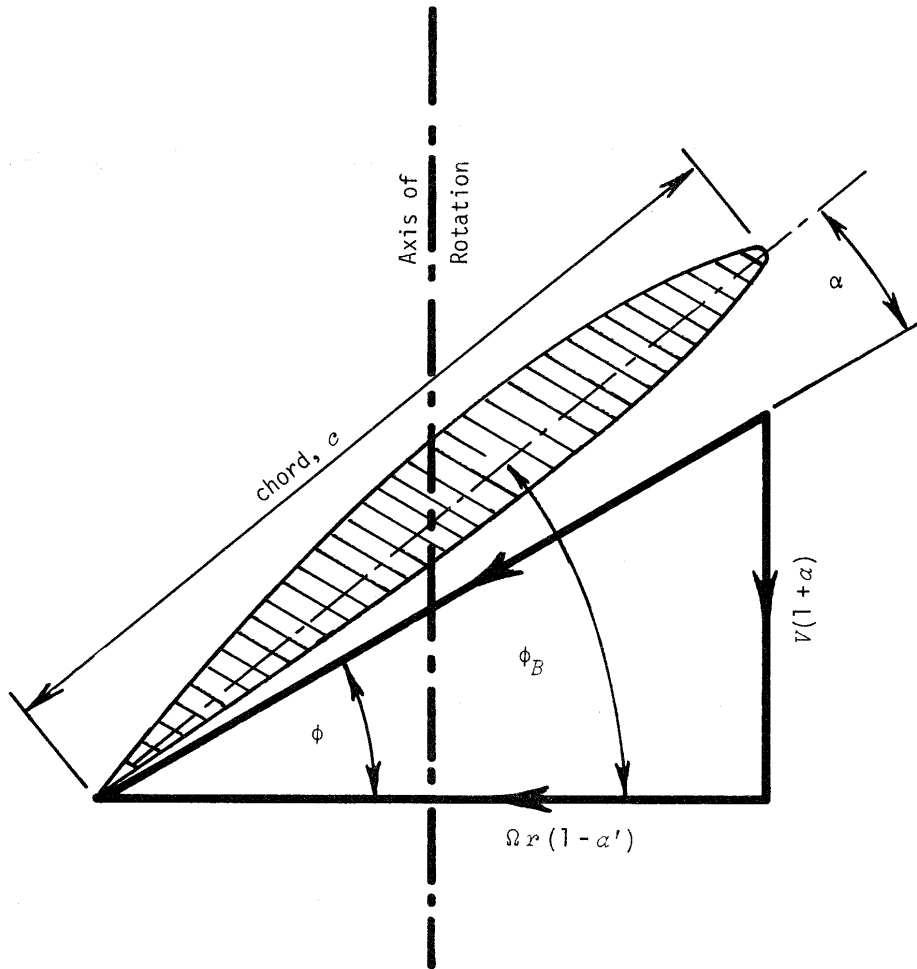


Fig. 7 Triangle of velocities at a blade section distance r from the axis of rotation.



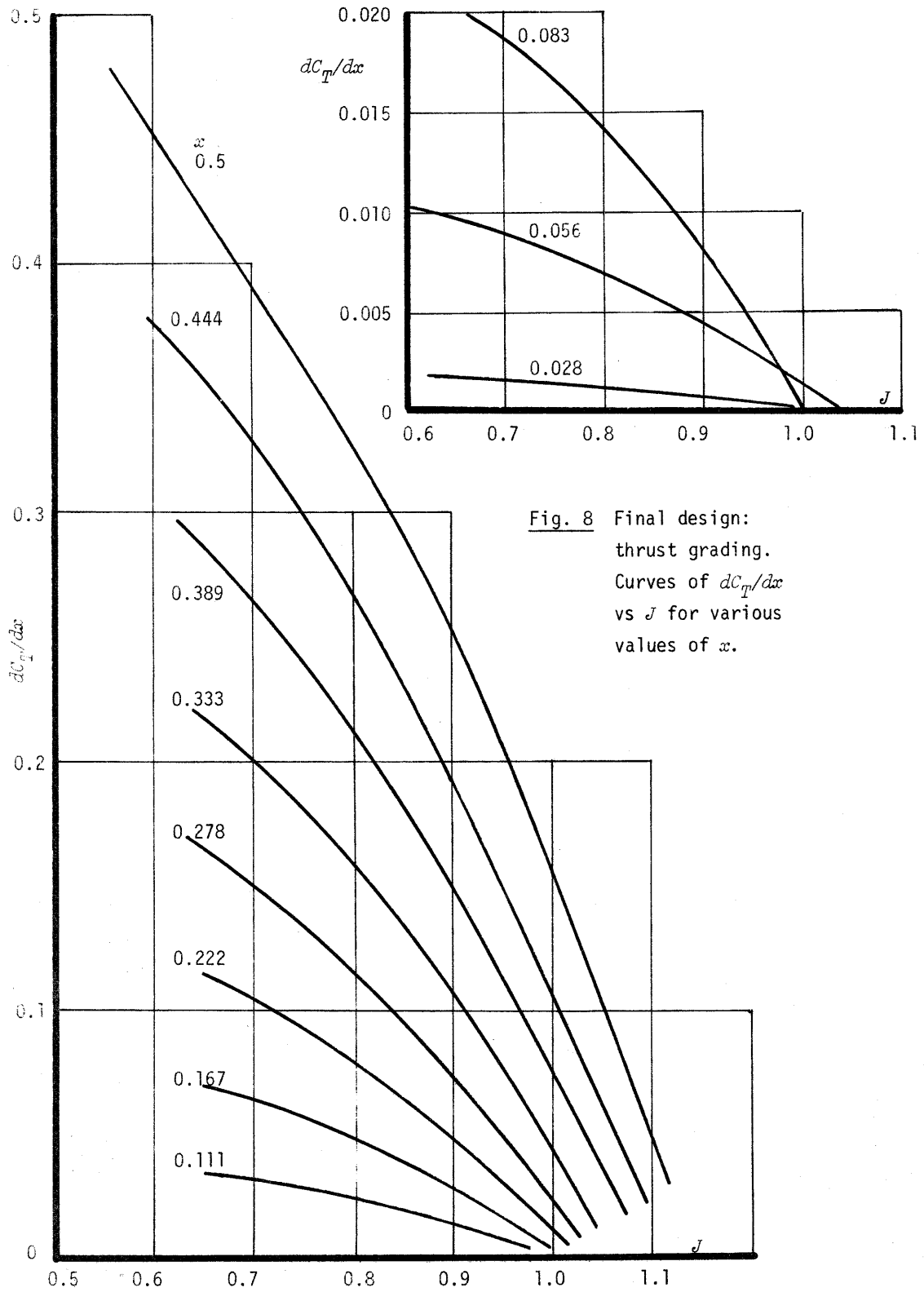


Fig. 8 Final design:
thrust grading.
Curves of dC_T/dx
vs J for various
values of x .

Fig. 9 Final design: thrust grading.
Curves of dC_T/dx vs x for
various values of J .

